Toward a measurement of α-decay lifetime change at high pressure: The case of ^{241}Am

Noaz Nissim,[1,*] Fabio Belloni,[2,†] Shalom Eliezer,[1,3] Domenico Delle Side,[4] and José Maria Martinez Val[3]
[1]*Applied Physics Division, Soreq NRC, Yavne, Israel*
[2]*European Commission, Directorate-General for Research and Innovation, Directorate Energy, Brussels, Belgium*
[3]*Nuclear Fusion Institute, Polytechnic University of Madrid, Madrid, Spain*
[4]*Department of Mathematics and Physics "Ennio De Giorgi", University of Salento, Lecce, Italy*
(Received 23 March 2016; published 1 July 2016)

This paper suggests that a change in the lifetime of the α-decay process in ^{241}Am may be detected at high pressures achievable in the laboratory, essentially, due to the extraordinary high compressibility of Am at the megabar range. The Thomas-Fermi model was used to calculate the effect of high pressure on the atomic electron density and the variation of the atomic potential of ^{241}Am. It was found that at pressures of about 0.5 Mbar the relative change in the lifetime of ^{241}Am is about -2×10^{-4}. Detailed experimental procedures to measure this effect by compressing the ^{241}Am metal in a diamond-anvil cell are presented where diagnostics is based on counting of the 60-keV γ rays accompanying the α decay and/or mass spectrometry on the ^{237}Np/^{241}Am isotope ratio.

DOI: 10.1103/PhysRevC.94.014601

I. INTRODUCTION

It is customary to treat the lifetime of radioactive elements as a constant of nature, although, already in the mid-20th century it was conjectured that it may be dependent on environmental conditions [1,2]. In their work, Segre [1] and Daudel [2] suggested that the lifetime associated with the radioactive processes of "electron capture" and "internal conversion" is proportional to the probability of the electrons being in the vicinity or inside the nuclei, respectively. This probability is evidently affected by the chemical surrounding of the atom. In the 1970s, a number of theoretical papers were considering the possibility of changes in α-decay lifetimes due to changes in the electric potential barrier caused by changes in the electrons' cloud density in the vicinity of the nuclei, i.e., electron screening [3–6]. In the years following these works, much was performed mainly in the direction of combining a radioactive element in a metallic matrix, allowing a chemical environment with an abundance of conducting electrons to enhance electron screening. Reference [7] reported on a 40% increase in lifetime for a β decay of ^{3}H in a Ti matrix. In Ref. [8] it was claimed that the lifetime was reduced by 6% for α decay of ^{210}Po in a Cu matrix. Also, many other works have been reported on changes of at most a few percent in the lifetime of α and β decays in different environmental conditions [9–15].

From a first glance, it seems that the lifetime of α decay should be less sensitive to environmental conditions than other radioactive decay processes, mainly due to the tens-MeV potential barrier. This large potential barrier may have played a major role in the current lack of experimental evidence for α-decay lifetime changes. Nevertheless, in the past decade there is an ongoing debate on the effect of extreme environmental conditions on the α-decay lifetime. In Refs. [16,17] it was claimed that at low temperatures, due to the Debye screening, the α-decay lifetime is shortened by 3 orders of magnitude. As a response, Ref. [18] and subsequent works [19–23] pointed out the unlikeliness of such a large effect due to a decrease in the α-particle energy along with the increase in the screening potential.

Understanding the effect of environmental conditions on the α-decay lifetime is appealing from several different aspects ranging from solving the nuclear waste problem [16] to achieving a deeper understanding of star formation and the relevant fusion processes in dense plasmas [17,24,25] to refining of cosmochronology [26].

Previously, we have calculated the effect of large compression on the α-decay lifetime using the Debye model for electron screening [27] and the superior Thomas-Fermi (TF) model [28]. It was found that a measureable effect can be achieved for static compressions available with a diamond-anvil cell (DAC). In this paper, we assess the feasibility of a measurement of the effect on the α decay of ^{241}Am at high pressure in a DAC. Following the screening of a number of possible candidate nuclides, ^{241}Am has turned out to be one of the most promising options due to among other things:

(1) its large compressibility which involves four phase transitions up to 0.5 Mbar,
(2) its simple decay scheme,
(3) its relatively low specific activity which softens radiation protection requirements in terms of DAC handling and shielding,
(4) the extremely long lifetime of the daughter nuclide, which keeps the γ spectrum *clean* against background and possible overlapping lines coming from the decay chain products.

II. THEORY

In the customary one-body model of the *bare* decay, the daughter nucleus and the α particle interact through a potential

*noaznissim@gmail.com
†fabio.belloni@ec.europa.eu

V_b, dependent only on their relative distance r,

$$V_b(r) = V_N(r) + V_C(r) + V_\ell(r), \tag{1}$$

where V_N is the attractive intranuclear potential, V_C is the Coulomb potential, and V_ℓ is the centrifugal potential associated with the relative angular momentum ℓ. After Buck *et al.* [29], we use the following expressions for .V_N, V_C, and V_ℓ:

$$V_N(r) = -V_0 \frac{1+\cosh(R/a)}{\cosh(r/a)+\cosh(R/a)}, \tag{2}$$

$$V_C(r) = \begin{cases} \frac{2(Z-2)e^2}{2R}\left[3-\left(\frac{r}{R}\right)^2\right], & r < R, \\ \frac{2(Z-2)e^2}{r}, & r \geqslant R, \end{cases} \tag{3}$$

$$V_\ell(r) = \frac{\hbar^2}{2\mu}\frac{\left(\ell+\frac{1}{2}\right)^2}{r^2}, \tag{4}$$

where Z is the atomic number of the parent nuclide, R and a are the radius and diffuseness of the nuclear potential, respectively, V_0 is the maximum depth of $V_N(r)$, μ is the reduced mass of the α-daughter system, and V_ℓ has been written in its Langer-modified form with $\ell(\ell+1)$ replaced by $(\ell+\frac{1}{2})^2$ to ensure consistency of the subsequently defined integrals, In this formalism, V_0 and a are global parameters whose values have been fixed by a fit at 162.3 MeV and 0.40 fm, respectively [29]. A plot of $V_b(r)$ is provided in Fig. 1 (continuous curve) for the α decay of ^{241}Am at $\ell = 0$.

In the semiclassical approximation, the decay width Γ_b is given by

$$\Gamma_b = (\hbar^2/4\mu)\, P_b\, F_b \exp(-2\, G_b), \tag{5}$$

where P_b is the α-particle preformation probability, the Gamow factor G_b is given by $G_b = \int_{r_1}^{r_2} k_b(r)\, dr$, and the normalization factor F_b is given by $F_b^{-1} = (1/2)\int_{r_0}^{r_1} k_b^{-1}(r)\, dr$. The wave number k_b is given by

$$k_b(r) = [(2\mu/\hbar^2)\,|V_b(r) - Q_b|]^{1/2}, \tag{6}$$

where Q_b is the total kinetic energy released in the decay and the classical turning points r_0, r_1, and r_2 ($r_0 < r_1 < R < r_2$) are the solutions of the equation $k_b(r) = 0$ (Fig. 1). The decay constant λ_b is given by $\Gamma_b/\hbar$; the lifetime τ_b is given by λ_b^{-1}.

The presence of a cloud of Z electrons around the parent nucleus gives rise to a local electron density $n(r)$ and an electron (*screening*) potential $V_e(r)$, linked through the Poisson equation. In our formalism, V_e is taken as the interaction potential with the (positive) elementary charge and is therefore a negative quantity. Here we assume that the electrons cannot penetrate into the nucleus, i.e., $n(r) = 0$ for $r < R$; accordingly, $V_e(r) = V_e(R)$ for $r < R$. In compressed matter, the electron cloud is customarily assumed to be confined into a Wigner-Seitz (WS) cell with radius $r_{\rm WS}$ within which global charge neutrality holds [i.e., $\int_R^{r_{\rm WS}} n(r) d^3r = Z$] [30]; $r_{\rm WS}$ is linked to the matter density ρ through the relation,

$$(4/3)\pi r_{\rm WS}^3 \rho = A_w/N_A, \tag{7}$$

where A_w is the atomic weight and N_A is the Avogadro number and ρ is in turn fixed by the compression factor $\eta \equiv \rho/\rho_0$, where ρ_0 is a reference (e.g., STP) density. The interaction potential V_b and the Q value are then modified as [28]

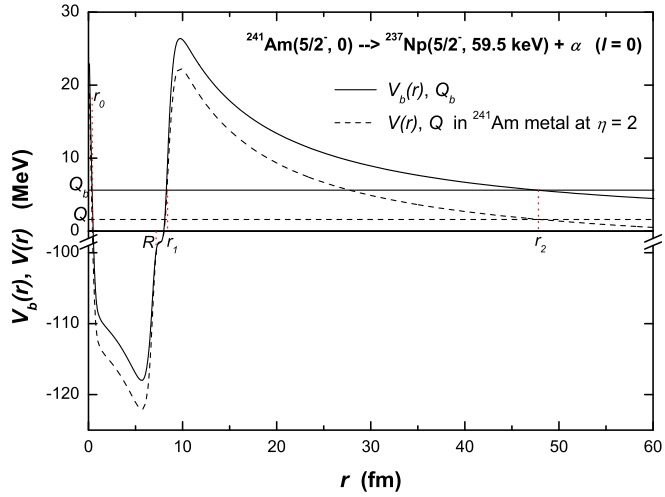

FIG. 1. Bare-nucleus and screened nuclear potentials in α-decay tunneling as a function of the daughter-nucleus or α-particle relative distance. Data refer to ^{241}Am; separation between the Q values and between the nuclear potential curves is magnified by a factor of 100.

$$V_b \to V(r) = V_b(r) + 2\, V_e(r), \tag{8}$$

$$Q_b \to Q = Q_b + \delta E_t, \tag{9}$$

where $\delta E_t \equiv E_{t,p} - E_{t,d} - E_{t,\alpha}$ and $E_{t,p}$, $E_{t,d}$, $E_{t,\alpha}$ are the total electron energies inside the WS cells of the parent, daughter, and He species, respectively. We have utilized the generalized TF model of the atom [31] to calculate $V_e(r)$ and δE_t upon compression as described in Ref. [28]. (Fundamentals of the TF theory for the compressed atom are given in Appendix A.) The electron-screened interaction potential $V(r)$ and the Q-value shift are shown in Fig. 1 (dashed lines) for the case of ^{241}Am.

Finally, lifetime variation has been calculated through the ratio,

$$\lambda/\lambda_b = (F/F_b)\exp\,[2(G_b - G)], \tag{10}$$

where λ, F, and G refer to the decay in the electron environment and no change in the α-preformation probability P_b has been assumed. The quantities F and G are built upon Eq. (6) as modified through the transformations in Eqs. (8) and (9). Values of $V_e(r)$ and δE_t calculated by means of the TF model are necessarily approximate, especially when quantum, exchange, and relativistic corrections are neglected; see Ref. [28] for extensive reliability considerations. Very briefly, the main issue is due to the fact that the TF model systematically overestimates the quantity $\delta V_e(r) = V_e(r) - V_e(R)$ in the tunneling region. Nevertheless, in Ref. [28] it is also shown that a reliable estimate of the lifetime variation can be obtained by taking the mean value of λ calculated between two limits of $\delta V_e(r)$: the upper one as given by the TF model and the lower one as given by $\delta V_e(r) \equiv 0$. This is also the way decay-width variations on Am-241 are calculated in the followings.

α decay of ^{241}Am (ground state, $T_{1/2} = 432.6y$) proceeds through several channels [32], each one with its own partial

TABLE I. Main α groups (i), branching ratios (b), and favored values of the relative angular momentum (ℓ) retained for calculation.

i	Decay levels[a] $[J^\pi, E(\text{keV})]$	B[a] (%)	ℓ[b]	Q[a,c] (keV)	Q_b[d] (keV)	R[e] (fm)
1	^{241}Am $(5/2^-,0) \rightarrow {}^{237}$Np	84.8	0	5637.8	5682.1	7.661
2	^{241}Am $(5/2^-,0) \rightarrow {}^{237}Np(7/2^-,102.96)$	13.1	2			

[a]From Ref. [32].
[b]Each branch is assumed to entirely occur in the state with the lowest possible value of ℓ. Higher-ℓ contributions to the variation of the partial decay width are negligible.
[c]Values for free atoms in their ground states.
[d]Values derived from Eq. (9) by using the free-atom Q value and δE_t. calculated from the binding-energy tables of Ref. [33]. The energy of the ith fed level of ^{237}Np is then subtracted in partial width calculations.
[e]From Ref. [29].

decay constant $\lambda_{b,i}$, and branching ratio B_i with $\lambda_b = \sum_i \lambda_{b,i}$ and $B_i = \lambda_{b,i}/\lambda_b$. Upon compression, $\lambda_b \rightarrow \lambda = \lambda_b + \delta\lambda$, where $\delta\lambda = \sum_i \delta\lambda_i$. It straightforwardly follows that

$$\frac{\delta\lambda}{\lambda_b} = \sum_i B_i \frac{\delta\lambda_i}{\lambda_{b,i}}. \tag{11}$$

Each term $\delta\lambda_i/\lambda_{b,i}$ can then be calculated according to the model described above.

We have considered only the two most intense α channels through which ^{241}Am disintegration takes place (Table I); by themselves, these two channels indeed account for about 98% of the decay width. Calculated values of $B_i\delta\lambda_i/\lambda_{b,i}$ and $\delta\lambda/\lambda_b$ are plotted as a function of η in Fig. 2. Nuclear parameters reported in Table I, along with host-matrix parameters $\rho_0 = 11.87$ g/cm^3, $A_w = 241.057$ g (^{241}Am metal) have been used for the calculation. Values of $\delta\lambda/\lambda_b$ are on the order of 10^{-3} in the compression domain $1 \leqslant \eta \leqslant 10$ and increase with compression, for instance, in matter at STP conditions ($\eta = 1$), we find $\delta\lambda/\lambda_b = 4.3 \times 10^{-3}$.

In the high-pressure experiment we propose, the decay constant variation $\delta\lambda$ is measured relative to the reference value λ_0 one finds in matter in ordinary conditions. In terms of the quantity $\delta\lambda/\lambda_b$ we have calculated, one finds straightforwardly,

$$\frac{\delta\lambda}{\lambda_0}(\eta) = \left[\frac{\delta\lambda}{\lambda_b}(\eta) - \frac{\delta\lambda}{\lambda_b}(1)\right]\left[1 + \frac{\delta\lambda}{\lambda_b}(1)\right]^{-1} \approx \frac{\delta\lambda}{\lambda_b}(\eta) - \frac{\delta\lambda}{\lambda_b}(1). \tag{12}$$

Values of $\delta\lambda/\lambda_0$ are plotted as a function of η in Fig. 2 as well. At the highest compression factors achievable in a DAC ($2 < \eta < 3$), $\delta\lambda/\lambda_0$ is on the order of 10^{-4}. We also note that $\delta\lambda/\lambda_0 > 0$ implies a reduction of lifetime upon compression.

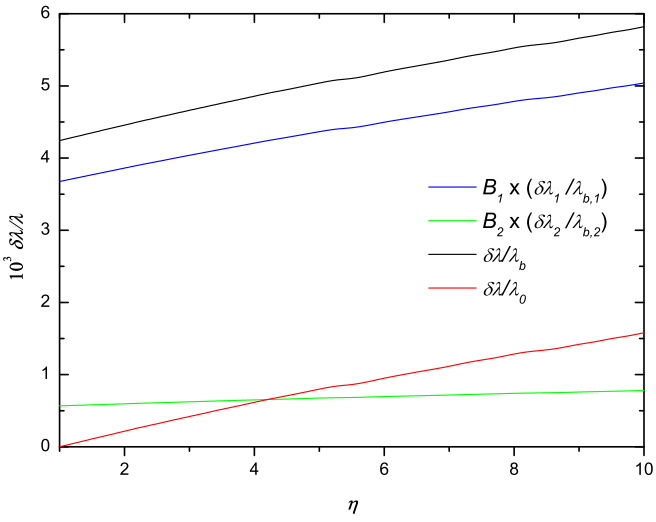

FIG. 2. Fractional variation of partial and total decay widths for ^{241}Am as a function of compression. Variations refer to the bare nucleus (λ_b) or matter at STP conditions (λ_0), respectively.

III. EXPERIMENTAL METHODS

A static high pressure can be produced by a DAC that can reach up to 1 Mbar. The α-decay rate can be determined by measuring the rate of the accompanied γ emission, especially when direct detection of the emitted α particles is not possible. If the extreme environmental conditions will impose instantaneous change in the lifetime of the parent nuclei, this will be instantaneously translated into a change in the γ-emission rate. Therefore, by measuring the γ-emission rate at different environmental conditions, the α-decay lifetime can be monitored. Alternatively, the α-decay rate can be retrieved by a mass-spectrometry measurement of the daughter-to-parent ratio in the sample after an adequate storage time.

In order to maximize the probability for a significant change in the lifetime of the source at high pressure, one of the essential properties of the α source should be that it undergoes a large volume change and preferably also a structural transition (usually followed, in turn, by a large and drastic volume change). It appears, that one such candidate can be ^{241}Am. The α decay in ^{241}Am is accompanied by the emission of 60-keV γ rays which are in the sensitivity range of a germanium detector. Furthermore, since Am is a synthetic material (made in nuclear reactors and not naturally present in the environment), at a narrow band measurement, the background readings should be very low. Static pressure experiments on metallic ^{243}Am [34] have shown that Am is compressed by a factor of 2 at a pressure of 0.5 Mbar after undergoing four phase transitions as can be seen in Fig. 3.

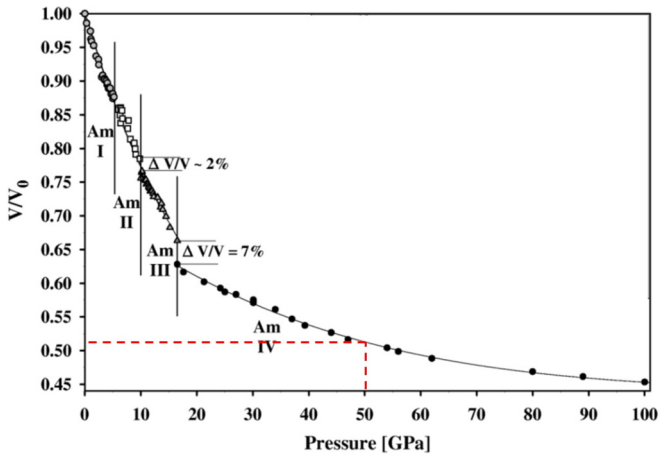

FIG. 3. Relative volume vs pressure curve for americium [34]. At 50 GPa the compression is about 2.

A. γ counting

We now estimate the γ-emission rate for our experimental setup. In Fig. 4, the inner part of a DAC is presented with typical dimensions of the sample volume for reaching 1 Mbar.

Assuming a ^{241}Am-metal point source with STP density of 11.87 g/cm^3, the maximum amount of Am that can be contained inside the sample volume is 1.86 μg. We will assume in our calculations a 1-μg source. The specific activity of ^{241}Am is 3.5 Ci/g, therefore in 1 μg there occur 1.3×10^5events/s. Since we are mainly interested in the 60-keV γ rays, which are emitted in only 36% of the events, we have a total of 46 800 relevant events/s. Assuming a detector with a $10 - \text{cm}^2$ effective detection area, located at about 5 cm from the source and with detection efficiency of 10%, we expect detection of $C = 150$ events/s.

The experiment is aiming at measuring the change in the half-life between a compressed and an uncompressed ^{241}Am sample. The small extent of the effect (see Sec. II), the relatively long half-life of ^{241}Am, as well as the limited counting rate make the application of Rutherford's differential method [35]—based on simultaneous monitoring of activity vs time of two different sources—and its versions [12,36] extremely challenging and of doubtful effectiveness as we have verified. In practice, one might rather attempt to perform the experiment by measuring the integrated activity of the uncompressed sample upon a certain defined time $\tilde{t}$, then compressing the sample and measuring the integrated activity for the same time $\tilde{t}$.

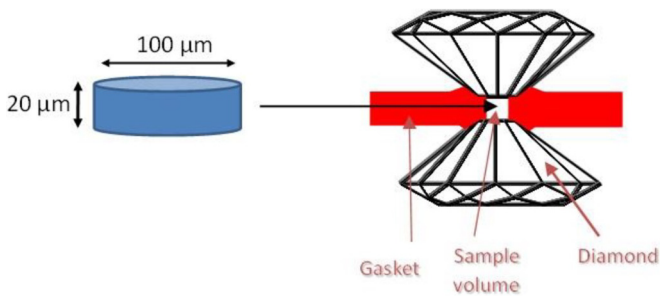

FIG. 4. The inner part of a DAC, and the sample volume dimensions for reaching 1 Mbar are presented on the left.

After a measurement time $\tilde{t}$, the number of counts from the uncompressed sample $N_0(\tilde{t})$ will be given by

$$N_0(\tilde{t}) = C\tilde{t}. \tag{13}$$

The statistical error of the measurement is $\Delta N_S(\tilde{t}) = \sqrt{N_0(\tilde{t})}$. At a compression factor of 2, we have calculated (Sec. II),

$$\frac{\delta\tau}{\tau_0} = -\frac{\delta\lambda}{\lambda_0} = -2.2 \times 10^{-4}. \tag{14}$$

The difference in the number of counts between the compressed and the uncompressed samples would then be as follows:

$$\delta N(\tilde{t}) = N(\tilde{t}) - N_0(\tilde{t}) = -2.2 \times 10^{-4}\, C\tilde{t}, \tag{15}$$

with an error,

$$\Delta\delta N(\tilde{t}) \cong \sqrt{2}\Delta N_S(\tilde{t}), \tag{16}$$

where $N(\tilde{t})$ is the total number of counts during the time $\tilde{t}$ for the compressed sample.

In order to be certain that we can detect the difference in counts as presented in Eq. (15), we demand this difference to be larger than the statistical error of the measurement, i.e.,

$$|\delta N(\tilde{t})| > \sqrt{2N(\tilde{t})}. \tag{17}$$

Following our estimates for ^{241}Am, we get

$$\tilde{t} > 76.5\ \text{h} > 3\ \text{days}.$$

We have utilized the useful approximation that C is the same for both the compressed and the uncompressed samples; this can be performed due to the long half-life of ^{241}Am. Nevertheless, an exact calculation can be performed to account for the change in C due to the time difference between the two measurements. We also note that C might be sensitive to setup-related effects induced by compression. Special attention should be paid to these possible sources of systematic errors in actual measurements.

1. Measurement systematic uncertainties

In the following subsections, we assess the main systematic effects affecting the measurement based on the comparison of the integral activities.

(a) Measurement uncertainty due to source-detector distance uncertainty. In Fig. 5, a one-detector measurement setup

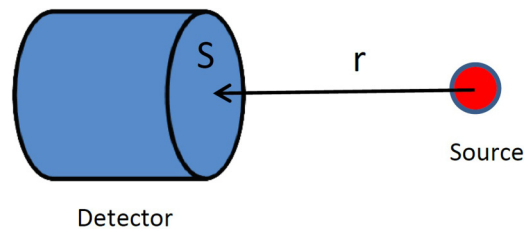

FIG. 5. One-detector setup.

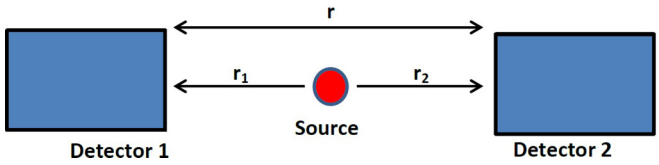

FIG. 6. Two-detector setup.

is presented. Assuming a point source with activity A, located at a distance r from a detector with a detection surface S, then the number of counts measured by the detector after a measurement time $\tilde{t}$ is (for a small-angle approximation),

$$N(\tilde{t},r) = \frac{A\tilde{t}S}{4\pi r^2}. \tag{18}$$

The differentiation of N with respect to r gives

$$\frac{dN(\tilde{t},r)}{dr} = -2\frac{N(\tilde{t},r)}{r}. \tag{19}$$

Therefore, the measurement relative error due to the uncertainty in the source-detector distance is as follows:

$$\frac{\Delta N_r}{N} = -2\frac{\Delta r}{r}. \tag{20}$$

Unlike the statistical error, the source-detector distance relative error does not decrease with N. For a sensitive measurement we require that

$$\left|\frac{\Delta N_r}{N}\right| \ll \left|\frac{\delta N}{N}\right| = 2.2\times 10^{-4}. \tag{21}$$

This implies $\Delta r \ll 5.5$ μm for $r = 5$ cm, which is a challenging procedure.

A more robust measurement setup would be the two-detector setup as presented in Fig. 6.

Assuming the two detectors have the same surface area S, the number of counts in each detector after time $\tilde{t}$ is as follows:

$$N_1 = \frac{A\tilde{t}S}{4\pi r_1^2}, \qquad N_2 = \frac{A\tilde{t}S}{4\pi r_2^2}, \tag{22}$$

where r_1 is the source-detector 1 distance and r_2 is the source-detector 2 distance and by assuming that both the detectors and the source are all confined to one axis we have $r = r_1 + r_2$.

The total number of counts in the two detectors is as follows:

$$N = N_1 + N_2 = G\left(\frac{1}{r_1^2} + \frac{1}{r_2^2}\right) = G\left(\frac{1}{r_1^2} + \frac{1}{(r-r_1)^2}\right),$$

$$G = \frac{A\tilde{t}S}{4\pi}. \tag{23}$$

Differentiating N with respect to r_1 gives

$$\frac{\Delta N_r}{\Delta r_1} = -2G\left(\frac{1}{r_1^3} - \frac{1}{r_2^3}\right). \tag{24}$$

And the relative error in the number of counts is therefore

$$\frac{\Delta N_r}{N} = -2\frac{\Delta r_1}{r_1}k, \qquad k = \left(\frac{r_2^3 - r_1^3}{r_2\left(r_2^2 + r_1^2\right)}\right). \tag{25}$$

If we require that the relative error in the number of counts will be much less than the expected measurement, for example, we take $|\Delta N_r/N| = 1\times 10^{-5}$, then the maximum acceptable error in the sample positioning is presented in Figs. 7 and 8.

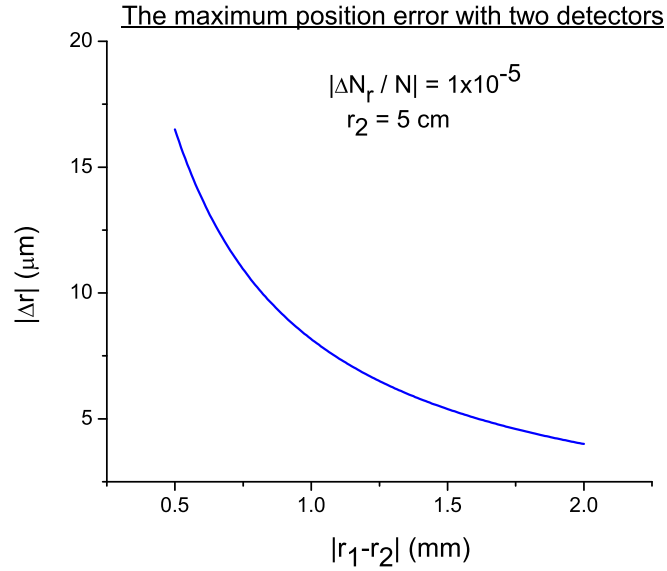

FIG. 7. Source-detector distance error vs the difference in distance between the two detectors. Detector 2 is located at a distance of 5 cm from the source, and the allowed relative error in the number of counts is 1×10^{-5}.

(b) Measurement uncertainty due to the ^{241}Am *self-absorption at 60 keV.* Self-absorption in radioactive sources is a well-known phenomenon, under continuous study to the present day. Contemporary research in the field is mainly concerned with determining the amount of radioactive material in radioactive waste. Already in 1948, Evans and Evans [37]

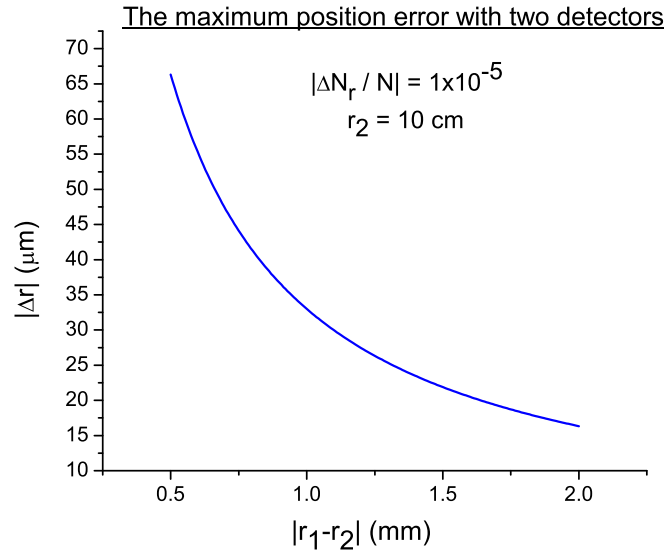

FIG. 8. Source-detector distance error vs the difference in distance between the two detectors. Detector 2 is located at a distance of 10 cm from the source, and the allowed relative error in the number of counts is 1×10^{-5}.

have calculated the self-absorption of radioactive sources in several geometries.

In the experiment proposed here, a cylindrical geometry (with uniform mass distribution) will be considered for the source as suggested by the DAC schematic in Fig. 4. Adapting the formulation for a linear source used in Ref. [31], we find that the self-absorption attenuation factor f_0 on the photon flux detected along the zenithal axis of a source of thickness l_0 and density ρ_0 is given to a very good approximation by

$$f_0 = \frac{1}{x_0}\left[1 - e^{-x_0} + \frac{2}{\mu_m \rho_0 r}(e^{-x_0} + x_0 - 1)\right], \qquad (26)$$

where $x_0 = \mu_m \rho_0 l_0$, μ_m is the mass absorption coefficient, and $l_0 \ll r$. One immediately recognizes that the following scaling holds upon compression: $f = f_0(\rho_0 \to \rho, l_0 \to l)$ with $\rho = \eta\rho_0, l = l_0\eta^{-1/3}$ (note that $x_0 \to x = x_0\eta^{2/3}$). For an ^{241}Am source with $l_0 = 10\ \mu$m, $\rho_0 = 11.87$ g/cm^3, and $\mu_m = 7.861$ cm^2/g at 60 keV [38], we find $\delta f/f_0 = -2.654 \times 10^{-2}$ at $\eta = 2$ and $r = 5$ cm.

(c) Measurement uncertainty due to the diamond absorption at 60 keV. The STP density of diamond is $\rho^D(0) = 3.518$ g/cm^3, and the density at 50 GPa is $\rho^D(50) = 3.86$ g/cm^3 [39]. The mass absorption coefficient of diamond is $\mu_m^D = 0.175$ cm^2/g [38]. In Fig. 9, the pressure distribution inside the diamond-anvil cell at 40 GPa is presented. It can be seen that about 10% of the diamond height is at the maximum pressure, and about 50% of the diamond height is under a pressure gradient from 40 GPa to about 10 GPa. For an estimate of the change in the absorption of the diamond, we will disregard the pressure gradients and assume only 10% of the diamond height is under maximum pressure.

Assuming that the diamond height is $h = 0.2$ cm and that a part of it, $h_P = 0.02$ cm, is at the maximum pressure in the diamond of 50 GPa, then the relative change in the photon intensity to the detector (i.e., the relative change in the anvil transmission $\delta a/a_0$) due to the change in the density of the diamond is given by

$$\frac{\delta a}{a_0} = 1 - \frac{e^{-\mu_m^D(h-h_P)\rho^D(0)} e^{-\mu_m^D h_P \rho^D(50)}}{e^{-\mu_m^D h \rho^D(0)}} = 1.0 \times 10^{-3}. \qquad (27)$$

Obviously, due to the pressure gradients in the diamond, this is a lower limit of the transmission change. An accurate *in situ* measurement of this quantity can be conducted with a 60-keV beam at a synchrotron.

(d) Measurement uncertainty due to the variation of the internal conversion coefficient of the 60-keV excited state of ^{237}Np. In general, compression also affects the internal conversion probability in nuclear transitions [4,36,40]. This also holds for ^{237}Np deexcitation. Unfortunately, no theoretical prediction or measurement of the effect in this case exists to date. In our experimental proposal, however, this effect might in turn impact on the photon flux to the detector upon compression so that an estimate is highly needed.

In detail, denoting by ε_0 the probability of photon emission from the 60-keV excited state of ^{237}Np and by α_0 the (total) internal conversion coefficient ($\alpha_0 = 1.16$ [32]), one has, by definition,

$$\varepsilon_0 = (1 + \alpha_0)^{-1}. \qquad (28)$$

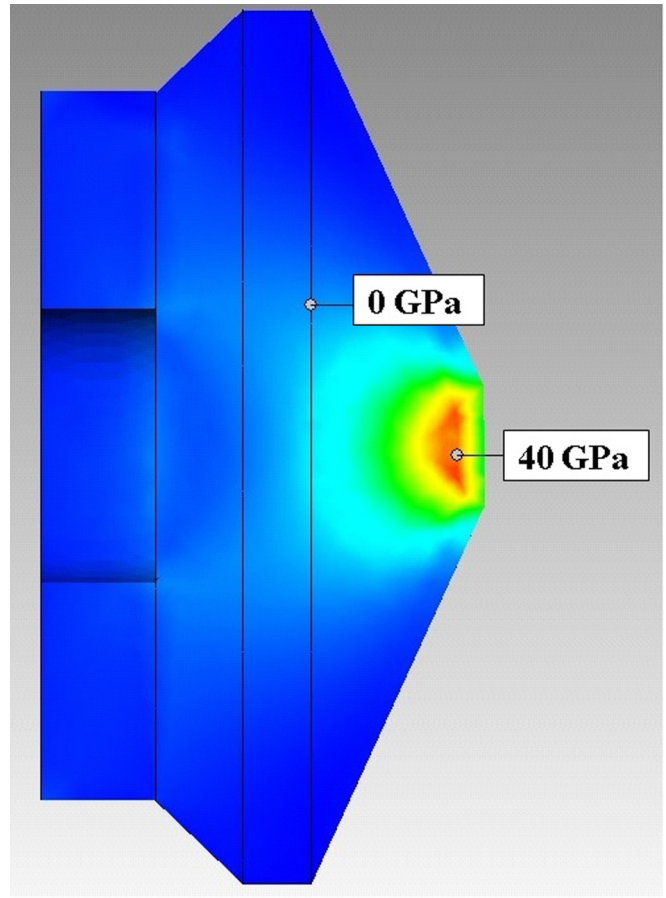

FIG. 9. A simulation of the pressure distribution inside a diamond-anvil cell at a sample pressure of 40 GPa. The red color represents the maximum pressure of 40 GPa, whereas the blue color represents 0 pressure.

From Eq. (28), it straightforwardly follows that, upon compression,

$$\delta\varepsilon/\varepsilon_0 = -\alpha_0\varepsilon_0(\delta\alpha/\alpha_0), \qquad (29)$$

where $\alpha_0\varepsilon_0 = 0.54$. For the purpose of calculating $\delta\alpha/\alpha_0$, one should follow the method described in Ref. [40], which is based on the explicit calculation of the matrix element of the multipole operator and involves electron wave functions of the compressed atom. Although rigorous, this method is computationally challenging, especially for high-Z nuclides and high transition energy. We have rather attempted a highly approximated estimate along the procedure described in Appendix B.

For ^{237}Np dispersed in an ^{241}Am matrix, we find $\delta\alpha/\alpha_0 \approx 1.5 \times 10^{-4}$ between $\rho_0 = 11.87$ g/cm^3 and $2\rho_0$. This results in $\delta\varepsilon/\varepsilon_0 \approx 8 \times 10^{-5}$. This figure is too imprecise and still too close to the expected value of $\delta\lambda/\lambda_0$ for the effect to be straightforwardly neglected.

2. Discussion

One generalizes Eq. (13) to take into account all the systematic uncertainties described in Secs. III A 1 a–III

A 1 d,

$$N_0 = M\frac{N_A}{A_w}\lambda_0\varepsilon_0 f_0 a_0 p_0, \tag{30}$$

where M is the source mass and we have denoted by p_0 the number of counts per unit source activity measured by the detector in the absence of in-medium attenuation as given by the ratio N/A in Eqs. (18) or (23). Equation (15) can then be rewritten as

$$\frac{\delta N}{N_0} \equiv \frac{N - N_0}{N_0} = \frac{\lambda\varepsilon f a p}{\lambda_0\varepsilon_0 f_0 a_0 p_0} - 1. \tag{31}$$

For ease of notation, indicating by y_ξ the generic quantity $\delta\xi/\xi_0$, Eq. (31) can in turn be rewritten in a more expressive fashion as

$$y_N = -1 + \prod_{\xi=\lambda,\varepsilon,f,a,p}(1 + y_\xi), \tag{32}$$

where $y_\lambda \sim 10^{-4}$ (Sec. II), $y_p \sim 10^{-5}$ (Sec. III A 1 a), $y_f = -2.654 \times 10^{-2}$ (Sec. III A 1 b), $y_a \cong -1.0 \times 10^{-3}$ (Sec. III A 1 c), and $|y_\varepsilon| \sim 10^{-5}$–$10^{-4}$ (Sec. III A 1 d).

In the lack of an accurate prediction of y_ε, we will conclude we could only be able to measure the combined effect of compression on the ^{241}Am α decay and ^{237}Np internal conversion.[1] These two quantities could be disentangled only by means of a complementary measurement, such as the mass-spectrometry determination of the ^{237}Np/^{241}Am isotope-ratio variation between the compressed and the uncompressed samples. This latter method is obviously insensitive to internal conversion; see Sec. III B. Hence, based solely on a measurement of y_N and the accurate knowledge of y_f, y_a, and y_p, one can retrieve the quantity $Y \equiv y_\lambda + y_\varepsilon$ from Eq. (32). Expanding the products and solving with respect to Y, one obtains

$$\begin{aligned} Y &\approx \left(y_N - \sum_{\xi=a,f,p} y_\xi\right)(1 + y_f)^{-1} \\ &\approx y_N - \sum_{\xi=a,f,p} y_\xi - y_N y_f + y_f^2, \end{aligned} \tag{33}$$

where terms on the order of 10^{-6} or smaller have been neglected.

Terms other than y_N on the right-hand side of Eq. (33) represent corrections we have to bring to our actual activity measurement in order to take setup-related systematic effects into account. If we encompass y_p directly into the error on Y, by associating with y_p a maximal error $\Delta y_p = y_p$, Eq. (33) then reduces to

$$Y \approx y_N - y_f - y_a - y_N y_f + y_f^2, \tag{34}$$

with the (absolute) error given by

$$(\Delta Y)^2 \approx \sum_{\xi=N,a,f,p}(\Delta y_\xi)^2 \tag{35}$$

[note that $(\partial Y/\partial y_\xi)^2 \approx 1$]. Equation (35) dramatically expresses further difficulties of our measurement, whose result is determined by the summation of terms of similar order of magnitude with different signs; indeed, y_N and y_f are on the order of 10^{-2}, y_a is on the order of 10^{-3}, and $y_N y_f$, y_f^2 are on the order of 10^{-4}.

We require $\Delta Y \sim 10^{-5}$, which implies that each term Δy_ξ in the summation of Eq. (35) has to be on the order of 10^{-5} or smaller. We finally note that:

(a) This requirement can somehow be achieved for Δy_p as discussed in Sec. III A 1 a.

(b) As for Δy_N, it is statistical in nature and can certainly be made as small as 10^{-5} (see Sec. III A). For $y_N \sim y_a \sim 10^{-3}$, this prescription requires a precise $\Delta y_N/y_N \sim 10^{-2}$, a level which can be reached for counting times of at least 1 month.

(c) As for Δy_f, it depends on the quantities l_0, ρ_0, ρ, r, and μ_m. One finds that the leading term in its calculation comes from the uncertainty on l_0; indeed, y_f is very sensitive to variations of l_0 and very little to variations of r. At the best of the experimental uncertainties (i.e., $\Delta\rho/\rho = \Delta\rho_0/\rho_0 = \Delta\mu_m/\mu_m = 0.001$, $\Delta r/r = \Delta l_0/l_0 = 0.01$) and with the same values of the parameters used in Sec. III A 1 b, Δy_f lowers down to 2.5×10^{-4}, a value which is as high as our estimate of y_λ. Moreover, the level of precision required on ρ is only achievable by means of a synchrotron-based measurement [41]. Indeed, in a standard DAC experiment where the pressure is evaluated with the ruby fluorescence method, it is customary to estimate the error in the pressure on the sample at 10% due to pressure gradients in the cell. In that case, the uncertainty in the density can be evaluated from the equation of state of the compressed material. For Am at 0.5 Mbar, a 10% error in pressure corresponds to about 2.5% uncertainty in the density.

(d) As for Δy_a with $y_a \sim 10^{-3}$, a precise $\Delta y_a/y_a \sim 10^{-2}$ is required in the prediction of the transmission change in the diamond. This level of precision can certainly be achieved via a direct measurement at a synchrotron.

B. Mass spectrometry

Neptunium-237 α decays to ^{233}Pa with a half-life of 2.144×10^6 yr which is also slightly affected by compression. Denoting by $\mathcal{R}_0(t)$ the ^{237}Np/^{241}Am ratio in the uncompressed sample at the time t, elapsed from the beginning of the experiment, and by $\lambda_{d,0}$ the decay constant of ^{237}Np, this ratio is given by the (general) relation [42],

$$\begin{aligned} \mathcal{R}_0(t) = &\frac{\lambda_0}{\lambda_0 - \lambda_{d,0}}\{\exp[(\lambda_0 - \lambda_{d,0})t] - 1\} \\ &+ \mathcal{R}_0^0 \exp[(\lambda_0 - \lambda_{d,0})t], \end{aligned} \tag{36}$$

[1]The situation is further complicated by the fact that $y_\lambda > 0$ whereas $y_\varepsilon < 0$, meaning that the induced variations in the α lifetime and in the conversion coefficient act in opposite directions on the photon flux, the former tending to increase it and the latter to reduce it.

where $\mathcal{R}_0^0 = \mathcal{R}_0(0)$. In the limits $\lambda_{d,0} \ll \lambda_0$ (indeed, $\lambda_{d,0}/\lambda_0 = 2 \times 10^{-4}$), $\lambda_0 t \ll 1$, and $\mathcal{R}_0^0 = 0$, Eq. (36) reduces to

$$\mathcal{R}_0(t) \approx \lambda_0 t + \tfrac{1}{2}(\lambda_0 t)^2 + \tfrac{1}{2}\lambda_0 \lambda_{d,0} t^2, \tag{37}$$

which is accurate up to the order of 10^{-10} for $t \sim 1$ yr and the lifetime values considered here. Differentiating Eq. (37) with respect to the lifetimes and assuming that $\delta\lambda_d/\lambda_{d,0} \sim \delta\lambda/\lambda_0 \sim 10^{-4}$, one easily finds that the fractional variation of the isotope ratio upon compression is expressed by the attractively simple relation,

$$\frac{\delta\mathcal{R}}{\mathcal{R}_0} \approx \frac{\delta\lambda}{\lambda_0}, \tag{38}$$

where terms on the order of 10^{-7} and smaller have been neglected for $t \sim 1$ yr. This simple equality can still be retained in the limit for the original purity of the samples $\mathcal{R}_0^0 \ll \lambda_0 t$.

Equation (38) states that, in our case, the fractional lifetime variation of the parent can be directly measured from the variation of the daughter-to-parent isotope ratio between the compressed and the uncompressed samples. This means, however, being able to measure $\mathcal{R}, \mathcal{R}_0$ with a precision better than 10^{-4}. Moreover, the isotope ratio is already a tiny quantity because after, e.g., 1 yr, $\mathcal{R}_0 = 1.6 \times 10^{-3}$ (note that stability of DACs can be kept even for several years at pressures on the order of magnitude considered in this study). High-precision high-sensitivity mass-spectrometry techniques are therefore needed; multi-collector-inductively-coupled-plasma mass spectrometry (MC-ICP-MS) [43] appears to be particularly suited to our case.

Assuming precision of the isotope ratio measurement is only determined by counting statistics, one can neglect the statistical uncertainty on the number of counts for ^{241}Am compared to the minority species ^{237}Np. The maximum level of achievable precision will then depend on the uncertainty on the ^{237}Np integral counting. The main limiting factor acting over this quantity is the amount of ^{237}Np occurring in the sample. Indeed, if we set at 1.0×10^{-4} the maximum acceptable uncertainty on $\delta\mathcal{R}/\mathcal{R}_0$, this translates into the requirement,

$$\left(\frac{\Delta\mathcal{R}_0}{\mathcal{R}_0}\right)^2 + \left(\frac{\Delta\mathcal{R}}{\mathcal{R}}\right)^2 = 1.0 \times 10^{-8}, \tag{39}$$

which leads to

$$\frac{\Delta\mathcal{R}}{\mathcal{R}} \approx \frac{1}{\sqrt{N_d}} = \frac{1}{\sqrt{2}} \times 10^{-4} \tag{40}$$

for $\Delta\mathcal{R}_0/\mathcal{R}_0 = \Delta\mathcal{R}/\mathcal{R}$, being N_d the number of ^{237}Np counts and having used the customary Poissonian statistical error.

Equation (40) yields $N_d = 2 \times 10^8$. Assuming a sample utilization (i.e., ratio of ions detected to atoms in solution consumed) on the order of 10^{-2} for state-of-the-art MC-ICP-MS instruments, at least 2×10^{10} ^{237}Np atoms are needed in each sample. This figure is well below the expected abundance of ^{237}Np in a 1-μg originally pure ^{241}Am sample after 1-yr storage, which can easily be estimated in 4×10^{12} atoms. Recoil-induced depletion of ^{237}Np (from decay kinematics) is absolutely negligible for the sample size considered here.

IV. CONCLUSION

Experimental procedures for measuring the change in the α-decay lifetime of ^{241}Am due to static high pressure were presented. The ^{241}Am metal provides a good candidate for detecting changes in α-decay lifetime at high pressures due to its large compressibility by a factor of about 2 at 0.5 Mbar. This compression includes four high-pressure phase transitions which occasionally results in drastic changes in the electronic structure of matter. In the proposed experimental setup the sample is compressed in a DAC suitable for reaching the megabar range.

To overcome the short mean-free path of the α particles in matter, the possibility of measuring the 60-keV γ-rays accompanying the α decay was considered. However, the small extent of the effect (our calculations predict a relative half-life change of about -2×10^{-4} for ^{241}Am at 0.5 Mbar), the relatively long half-life of ^{241}Am, as well as the limited counting rate achievable make the application of a differential activity-vs-time measurement impractical. On the other hand, a measurement based on time-integrated γ counting would be affected by heavy systematic uncertainties (a detailed analysis was provided), which makes this option not feasible upon the given prediction of the extent of the effect.

Nevertheless, one has to consider that the TF model was used to calculate atomic quantities relevant to the variation of the α-decay potential barrier and Q value. For this purpose and within the approximations of this study, it was previously [28] shown that TF calculations can provide acceptable results in the domain of relatively moderate compressions. However, we believe that the TF approximation provides a lower limit to the possible change in the α-decay lifetime since a more detailed (quantum) calculation should also include the increase in the s-electrons' density in the nucleus with pressure as is well known from Mössbauer spectroscopy measurements [44,45]. An effect of higher extent, up to the order of 10^{-3}, does not appear to be unlikely.

Finally, we showed that, even at the level of the current estimate, a mass-spectrometry measurement based on the variation of the ^{237}Np/^{241}Am ratio upon compression after a decay time on the order of 1 yr, is feasible. Conclusions here drawn for ^{241}Am actually have a wider scope since they can straightforwardly be extended to other candidate nuclides with similar characteristics.

APPENDIX A: FUNDAMENTALS OF THE TF MODEL

In this appendix, a few basic equations of the TF model of the atom [31] are presented, which are instrumental to concepts and calculations of Sec. II and Appendix B.

In the limit $T = 0$, atomic electrons constitute a degenerate fluid whose density of states in the phase space is given by [46]

$$\frac{dn(r)}{d^3p} = \frac{2}{h^3}, \tag{A1}$$

where $n(r)$ is the spatial density introduced in Sec. II, $\boldsymbol{p}$ is the momentum, h is the Planck constant, and the factor 2 is due to spin degeneracy. At a given point $\boldsymbol{r}$, electrons feel the atomic

potential $V_a(r)$, linked to $V_e(r)$ through the relation,

$$V_a(r) = -Ze^2/r - V_e(r), \tag{A2}$$

and fill every energy level E between $E_{\min} = V_a(r)$ and $E_{\max} = M$, where M is the chemical potential ($M = 0$ for the free atom, $M > 0$ for the compressed atom). Consequently, p varies according to the basic relation,

$$\frac{p^2}{2m} + V_a(r) = E, \tag{A3}$$

where m is the electron mass. By integrating dn/dp between $p_{\min} = 0$ and $p_{\max} = \sqrt{2m[M - V_a(r)]}$, one obtains

$$n(r) = C_n[M - V_a(r)]^{3/2}, \tag{A4}$$

where $C_n = (8/3)\pi(2m)^{3/2}h^{-3}$.

For the purpose of self-consistently calculating $V_a(r)$, one applies Poisson's equation with $n(r)$ given by Eq. (A4). It is then derived that V_a can be calculated in terms of a screening function ϕ, through the relation,

$$M - V_a(r) = (Ze^2/r)\phi(x), \tag{A5}$$

where $x = r/\Lambda$, $\Lambda = 0.88534a_0Z^{-1/3}$, and a_0 is the Bohr radius. The function $\phi(x)$ is the solution of the differential equation (*TF equation*),

$$\phi'' = x^{-1/2}\phi^{3/2}, \tag{A6}$$

with the boundary conditions,

$$\phi(0) = 1, \tag{A7}$$

and

$$\phi(x_{\rm WS}) - x_{\rm WS}\phi'(x_{\rm WS}) = 0 \tag{A8}$$

for atoms in compressed matter.[2] The chemical potential is determined via Eq. (A5), calculated at the boundary $r = r_{\rm WS}$, where $V_a = 0$.

In terms of ϕ, $V_e(r)$ is finally calculated as

$$V_e(r) = (Ze^2/r)[\phi(x) - 1] - M. \tag{A9}$$

The total electron energy E_t is calculated, in terms of ϕ, as $E_t = E_k + E_p$, with the kinetic energy E_k and the potential energy E_p given by

$$E_k = C_k \int_0^{r_{\rm WS}} n^{5/3}(r)d^3r,$$
$$E_p = (1/2)\int_0^{r_{\rm WS}} n(r)[V_a(r) - Ze^2/r]d^3r, \tag{A10}$$

where $C_k = 2.1884 \times 10^{-18}$ keV cm^2 and Eqs. (A4) and (A5) are to be used.

[2]Calculations in Sec. II have actually been performed by using an *ad hoc* boundary condition at $x = R$ in place of Eq. (A7). The interested reader is addressed to Ref. [28] for details.

APPENDIX B: A SIMPLIFIED METHOD TO ESTIMATE THE VARIATION OF THE INTERNAL CONVERSION COEFFICIENT

In connection to the problem of estimating the variation of the internal conversion coefficient by the effect of compression considered in Sec. III A 1 d, we have developed a simple approximate computational method, based on semiclassical arguments and the use of the TF model of the atom, which we present in this Appendix.

On the basis of nonrelativistic point-like-nucleus calculations, partial conversion coefficients for principal quantum numbers and electric or magnetic nuclear transitions of multipolarity order L and energy $\mathcal{E}$ are proportional to the electron density at the nucleus of the atomic shell involved, the proportionality factor being approximately dependent only on the electromagnetic character of the transition, L, and $\mathcal{E}$ [47]. Thanks to the additivity property of the partial coefficients, we then assume that the total conversion coefficient α is proportional to the overall density at the nucleus of the electrons having binding energies lower than $\mathcal{E}$. Indicating this electron density with $n_{\mathcal{E}}(0)$, upon compression, we write with the notation of previous sections,

$$\frac{\delta\alpha}{\alpha_0} = \frac{\delta n_{\mathcal{E}}(0)}{n_{\mathcal{E},0}(0)} \equiv \frac{n_{\mathcal{E}}(0)}{n_{\mathcal{E},0}(0)} - 1. \tag{B1}$$

We use the TF model to estimate the ratio $n_{\mathcal{E}}(0)/n_{\mathcal{E},0}(0)$. Although it is well known that the $r^{-3/2}$ divergence of $n(r)$ for $r \to 0$ is one of the main drawbacks of the TF model [48] [actually, we find that $n_{\mathcal{E}}(r) \sim r^{-1/2}$ for $r \to 0$], we will show, however, that the ratio $n_{\mathcal{E}}(0)/n_{\mathcal{E},0}(0)$ is well defined.

We will first find $n_{\mathcal{E}}(r)$. With a procedure analog to that used in Appendix A to derive Eq. (A4) from Eq. (A1), we consider electrons with energy ranging from

$$E_{\min} = E_{\min}(r) = \begin{cases} -\mathcal{E}, & V_a(r) \leqslant -\mathcal{E}, \\ V_a(r), & V_a(r) > -\mathcal{E}, \end{cases} \tag{B2}$$

to $E_{\max} = M$ and integrate dn/dp between

$$p_{\min} = \begin{cases} \sqrt{-2m[\mathcal{E} + V_a(r)]}, & V_a(r) \leqslant -\mathcal{E}, \\ 0, & V_a(r) > -\mathcal{E}, \end{cases} \tag{B3}$$

and $p_{\max} = \sqrt{2m[M - V_a(r)]}$. After some algebra, we obtain

$$n_{\mathcal{E}}(r) = n(r)C_{\mathcal{E}}(r), \tag{B4}$$

where

$$C_{\mathcal{E}}(r) = \begin{cases} 1 - \left[1 - \frac{\mathcal{E}+M}{M-V_a(r)}\right]^{3/2}, & V_a(r) \leqslant -\mathcal{E}, \\ 1, & V_a(r) > -\mathcal{E}, \end{cases} \tag{B5}$$

and $n(r)$ is given by Eq. (A4).

After noticing that, for $r \to 0$, $V_a(r) \sim -Ze^2/r$, hence $n(r) \sim C_n(Ze^2)^{3/2}r^{-3/2}$ and $C_{\mathcal{E}}(r) \sim (3/2)(Ze^2)^{-1}(\mathcal{E} + M)r$, we find

$$\frac{n_{\mathcal{E}}(0)}{n_{\mathcal{E},0}(0)} = \frac{\mathcal{E} + M}{\mathcal{E} + M_0}. \tag{B6}$$

In typical cases, $M \sim M_0 \ll \mathcal{E}$; we finally obtain

$$\frac{\delta\alpha}{\alpha_0} \approx \frac{\delta M}{M_0}\frac{M_0}{\mathcal{E}}. \tag{B7}$$

We have benchmarked our result against the well-known case of the 2-keV $E3$ isomeric transition of ^{99}Tc compressed to $\eta = 1.1$ [36,40,49]. We calculate (see Appendix A) $M = 19.69$ and $M_0 = 17.88$ eV (at $r_{\mathrm{WS},0} = 2.84a_0$ [40]), which yields $\delta\alpha/\alpha_0 = 9.0 \times 10^{-4}$ for $\mathcal{E} = 2.173$ keV. This figure is to be compared with the value of 4.6×10^{-4} measured by Mazaki *et al.* [36] as well as the quantum-mechanical value of 2.3×10^{-4} calculated by Porter and McMillan [40]. Although oversimplified, our method seems to be capable of at least providing an estimate on the order of magnitude of the effect.

For the 60-keV $E1$ transition of ^{237}Np dispersed into a compressed ^{241}Am matrix, we calculate[3] $M = 19.22$ eV at $\eta = 2$ and $M_0 = 9.10$ eV at $\rho_0 = 11.87$ g/cm^3, which yields $\delta\alpha/\alpha_0 = 1.5 \times 10^{-4}$ for $\mathcal{E} = 59.54$ keV.

[3]For extremely diluted dispersions of this kind, the chemical potential is actually imposed by the majority species.

[1] E. Segre, Phys. Rev. **71**, 274 (1947).
[2] R. Daudel, Rev. Sci. **85**, 162 (1947).
[3] H. Mazaki, J. Phys. E: Sci. Instrum. **11**, 739 (1978).
[4] G. T. Emery, Annu. Rev. Nucl. Sci. **22**, 165 (1972).
[5] W. Rubinson and M. L. Perlman, Phys. Lett. B **40**, 352 (1972).
[6] K. Alder, G. Baur, and U. Raff, Phys. Lett. A **34**, 163 (1971).
[7] O. Reifenschweiler, Phys. Lett. A **184**, 149 (1994).
[8] F. Raiola, T. Spillane, B. Limata, B. Wang, S. Yan, M. Aliotta, H. W. Becker, J. Cruz, M. Fonseca, L. Gialanella, A. P. Jesus, K. U. Kettner, R. Kunze, H. Luis, J. P. Ribeiro, C. Rolfs, M. Romano, D. Schurmann, and F. Strieder, Eur. Phys. J. A **32**, 51 (2007).
[9] B. Wang, S. Yan, B. Limata, F. Raiola, M. Aliotta, H. W. Becker, J. Cruz, N. De Cesare, A. D'Onofrio, Z. Fulop, L. Gialanella, G. Gyurky, G. Imbriani, A. Jesus, J. P. Ribeiro, V. Roca, D. Rogalla, C. Rolfs, M. Romano, D. Schurmann, E. Somorjai, F. Strieder, and F. Terrasi, Eur. Phys. J. A **28**, 375 (2006).
[10] B. Limata, F. Raiola, B. Wang, S. Yan, H. W. Becker, A. D'Onofrio, L. Gialanella, V. Roca, C. Rolfs, M. Romano, D. Schurmann, F. Strieder, and F. Terrasi, Eur. Phys. J. A **28**, 251 (2006).
[11] T. Spillane, F. Raiola, F. Zeng, H. W. Becker, L. Gialanella, K. U. Kettner, R. Kunze, C. Rolfs, M. Romano, D. Schurmann, and F. Strieder, Eur. Phys. J. A **31**, 203 (2007).
[12] L. Liu and C. Huh, Earth Planet. Sci. Lett. **180**, 163 (2000).
[13] A. Ray, P. Das, S. K. Saha, S. K. Das, B. Sethi, A. Mookerjee, C. Basu Chaudhuri, and G. Pari, Phys. Lett. B **455**, 69 (1999).
[14] H. Jeppesen, J. Byskov-Nielsen, P. Wright, J. G. Correia, L. M. Fraile, H. O. U. Fynbo, K. Johnston, and K. Riisager, Eur. Phys. J. A **32**, 31 (2007).
[15] P. Pöml, F. Belloni, E. D'Agata, E. Colineau, A. Morgenstern, J.-C. Griveau, V. V. Rondinella, R. Repnow, V. Nassisi, P. B. J. M. Benneker, J.-M. Lapetite, and J. Himbert, Phys. Rev. C **89**, 024320 (2014).
[16] K. U. Kettner, H. W. Becker, and C. Rolfs, J. Phys. G: Nucl. Part. Phys. **32**, 489 (2006).
[17] C. Rolfs, Prog. Part. Nucl. Phys. **59**, 43 (2007).
[18] N. T. Zinner, Nucl. Phys. **A781**, 81 (2007).
[19] Z. Patyk, H. Geissel, Y. A. Litvinov, A. Musumarra, and C. Nociforo, Phys. Rev. C **78**, 054317 (2008).
[20] F. F. Karpeshin, Phys. Rev. C **87**, 054319 (2013).
[21] S. Igashov and Y. M. Tchuvil'sky, Phys. At. Nucl. **76**, 1452 (2013).
[22] A. Y. Dzyublik, Phys. Rev. C **90**, 054619 (2014).
[23] N. Wan, C. Xu, and Z. Ren, Phys. Rev. C **92**, 024301 (2015).
[24] H. Assenbaum, K. Langanke, and C. Rolfs, Z. Phys. A: At. Nucl. **327**, 461 (1987).
[25] J. Cruz, Z. Fülöp, G. Gyürky, F. Raiola, A. Di Leva, B. Limata, M. Fonseca, H. Luis, D. Schürmann, M. Aliotta, H. W. Becker, A. P. Jesus, K. U. Kettner, J. P. Ribeiro, C. Rolfs, M. Romano, E. Somorjai, and F. Strieder, Phys. Lett. B **624**, 181 (2005).
[26] J. Su, Z. H. Li, L. C. Zhu, G. Lian, X. X. Bai, Y. B. Wang, B. Guo, B. X. Wang, S. Q. Yan, S. Zeng, Y. J. Li, E. T. Li, S. J. Jin, X. Liu, Q. W. Fan, J. L. Zhang, X. Y. Jiang, J. X. Lu, X. F. Lan, X. Z. Tang, and W. P. Liu, Eur. Phys. J. A **46**, 69 (2010).
[27] S. Eliezer, J. Martinez Val, and M. Piera, Phys. Lett. B **672**, 372 (2009).
[28] F. Belloni, Eur. Phys. J. A **52**, 32 (2016).
[29] B. Buck, A. C. Merchant, and S. M. Perez, At. Data Nucl. Data Tables **54**, 53 (1993).
[30] J. C. Pain, Phys. Lett. A **362**, 120 (2007).
[31] S. Eliezer, A. Ghatak, H. Hora, and E. Teller, *Fundamentals of Equations of State* (World Scientific, Hackensack, NJ, 2002).
[32] M. S. Basunia, Nucl. Data Sheets **107**, 2323 (2006).
[33] G. C. Rodrigues, P. Indelicato, J. P. Santos, P. Patté, and F. Parente, At. Data Nucl. Data Tables **86**, 117 (2004).
[34] S. Heathman, R. G. Haire, T. Le Bihan, A. Lindbaum, K. Litfin, Y. Méresse, and H. Libotte, Phys. Rev. Lett. **85**, 2961 (2000).
[35] E. Rutherford, Sitzber. Akad. Wiss. Wien. Math.-Naturw. Kl. **120**, 303 (1911).
[36] H. Mazaki, T. Nagatomo, and S. Shimizu, Phys. Rev. C **5**, 1718 (1972).
[37] R. D. Evans and R. O. Evans, Rev. Mod. Phys. **20**, 305 (1948).
[38] NIST XCOM data base, "http://physics.nist.gov/PhysRefData/Xcom/html/xcom1.html".
[39] A. Dewaele, F. Datchi, P. Loubeyre, and M. Mezouar, Phys. Rev. B **77**, 094106 (2008).
[40] R. A. Porter and W. G. McMillan, Phys. Rev. **117**, 795 (1960).
[41] A. Dewaele, P. Loubeyre, and M. Mezouar, Phys. Rev. B **70**, 094112 (2004).

[42] J. Magill and J. Galy, *Radioactivity, Radionuclides, Radiation* (Springer, Berlin, 2005).
[43] M. E. Wieser and J. B. Schwieters, Int. J. Mass Spectrom. **242**, 97 (2005).
[44] R. Ingalls, Phys. Rev. **155**, 157 (1967).
[45] J. A. Moyzis and H. G. Drickamer, Phys. Rev. **171**, 389 (1968).
[46] R. M. Moore, in *Nuclear Fusion by Inertial Confinement*, edited by G. Velarde, Y. Ronen, and J. M. Martinez Val (CRC, Boca Raton, FL, 1993).
[47] K. S. Krane, *Introductory Nuclear Physics* (Wiley, New York, 1988).
[48] O. J. Heilmann and E. H. Lieb, Phys. Rev. A **52**, 3628 (1995).
[49] K. T. Bainbridge, Chem. Eng. News **30**, 654 (1952).